Journal of Materials Chemistry A

Accepted Manuscript

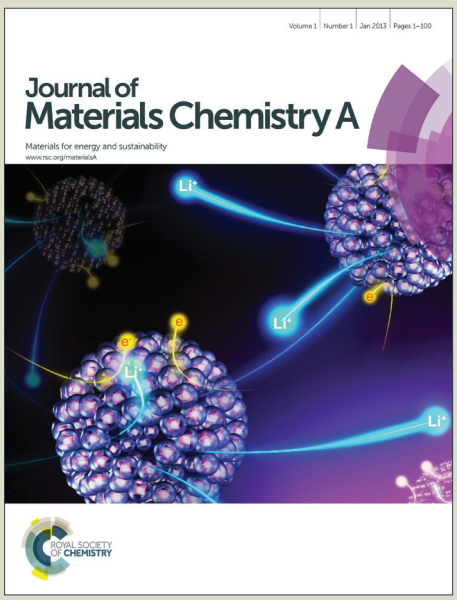

ROYAL SOCIETY OF CHEMISTRY

www.rsc.org/materialsA

Journal Name

RSCPublishing

ARTICLE

Highly reduced molybdophosphate as noble-metal-free catalyst for the reduction of chromium using formic acid as reducing agent

Kaining Gong[a], Weijie Wang[a], Jinshuang Yan[a], Zhangang Han*[,a]

Cite this: DOI: 10.1039/x0xx00000x

Received 00th January 2012,
Accepted 00th January 2012

DOI: 10.1039/x0xx00000x

www.rsc.org/

Highly reduced molybdophosphates with the formula $(H_2bpp)_6\{Co[Mo_6O_{12}(OH)_3(HPO_4)_3(H_2PO_4)]_2\}_2\cdot 13H_2O$ (**1**), $(H_2bpp)_6[Co(H_2O)_2]_4\{Co[Mo_6O_{12}(OH)_3(HPO_4)_2(H_2PO_4)(PO_4)]_2\}_2\cdot 2(HPO_4)\cdot 12H_2O$ (**2**), $[Na(H_2O)]_2[Co(mbpy)(H_2O)_3]_2[Co(mbpy)(H_2O)]_2\{Co[Mo_6O_{12}(OH)_3(HPO_4)_3(PO_4)]_2\}\cdot 8H_2O$ (**3**), and $Na_2[Co(mbpy)(H_2O)_3]_4\{Co[Mo_6O_{12}(OH)_3(HPO_4)_3(PO_4)]_2\}\cdot 13H_2O$ (**4**) (bpp = 1,3-bi(4-pyridyl)propane, mbpy = 5,5'-dimethyl-2,2'-dipyridyl) have been constructed and characterized. The primary structure of anionic moiety in **1-4** consists of Co(II) ion bridging two highly reduced $[P_4Mo^V_6O_{28}(OH)_3]^{9-}$ ($\{P_4Mo_6\}$) units into the hourglass-shape $\{Co(P_4Mo_6)_2\}$ cluster. Four supramolecular assemblies are of isomers and polymorphs with the difference in organic moieties: flexible bpp for **1-2** and chelated mbpy for **3-4**, revealing that pH values play important roles during the assembling process of hybrids. Electrochemical and catalytic properties of these hybrids are investigated. The preliminary experiments show that this type of hybrid system is active for electron transfer reaction of chromium(VI) reduction using formic acid at ambient temperature. Experimental results indicate that the reduction reaction can be carried out in a heterogeneous system with the lower reaction temperature and shorter reaction time. This kind of hybrid materials is easy to prepare and structurally design, and has the potential to replace precious metals Pt/Pd nanoparticles used in this field.

1. Introduction

The design and assembly of polyoxometalate (POM)-based supramolecular hybrids is an appealing subject due to not only their fascinating structural diversities, but also their potential applications in catalysis, absorption, electrochemistry and materials science.[1-5] The formation and crystallization of POMs is greatly contingent on several reaction conditions, such as pH value, temperature, starting material, ratio of initial reagent, which have an influence on the final product and their topological structures. As one important branch in POM family, the hourglass-shape polyoxomolybdenum phosphates consisting of two $[P_4Mo^V_6O_{31}]^{12-}$ ($\{P_4Mo_6\}$) linked by a metal ion, have attracted great interest because of the highly reduced cluster itself. In polyanion, the central metals are not only acting as the counter ions but also as the bridging units to connect two $\{P_4Mo_6\}$.[6] More importantly, the transition-metal centers can influence on the microstructure and physicochemical property of target product. So far, many metal ions including iron, cobalt, nickel, zinc, cadmium, and manganese centers, have been introduced into this system.[7-10]

POM-based hybrid materials with the structural integrity in some common solvents can be used as the recovering and recycle catalytic materials for many reactions, namely, facilitating catalytic process changing from homogeneous to heterogeneous. Organic parts are usually considered to be as structure-directing reagents to control the final structure of hybrids, as organic ligands to take part in the coordination and bridge inorganic fragments, as well as the charge-compensating cations to balance system.[11] Leroy Cronin' and Yan Xu' groups have reported many molybdenum phosphates and well discussed organoamines' structure-directing reagent effect in synthesis.[11,12] Our recent research has focused on the synthesis of POM-based supramolecular assemblies. Such hybrid systems can potentially combine the advantages of inorganic oxo-metal clusters and organic molecules, as well as benefit from close interaction and synergistic effect between two moieties.[13] This work is to explore the internal affection of organoamine templates on the self-assembly of reduced polyoxomolybdenum phosphate. Cobalt-containing molybdophosphate-based hybrids: $(H_2bpp)_6\{Co[Mo_6O_{12}(OH)_3(HPO_4)_3(H_2PO_4)]_2\}_2\cdot 13H_2O$ (**1**), $(H_2bpp)_6[Co(H_2O)_2]_4\{Co[Mo_6O_{12}(OH)_3(HPO_4)_2(H_2PO_4)(PO_4)]_2\}_2\cdot 2(HPO_4)\cdot 12H_2O$ (**2**), $[Na(H_2O)]_2[Co(mbpy)(H_2O)_3]_2[Co(mbpy)(H_2O)]_2\{Co[Mo_6O_{12}(OH)_3(HPO_4)_3(PO_4)]_2\}\cdot 8H_2O$ (**3**) $Na_2[Co(mbpy)(H_2O)_3]_4\{Co[Mo_6O_{12}(OH)_3(HPO_4)_3(PO_4)]_2\}\cdot 13H_2O$ (**4**) (bpp = 1,3-bi(4-pyridyl)-propane; mbpy = 5,5'-dimethyl-2,2'-dipyridyl) have been constructed and characterized. This kind of hybrid systems with reduced polyanionic cluster could

be used in environmental cleanup, such as the removal of Cr(VI) from wastewater.

Among various water pollutants, hexavalent Cr is one of the most toxic, mutagenic, and carcinogenic components, and must be required removal from water at any cost.[14-18] EPA maximum total chromium contaminant level for drinking water is 0.1 mg L^{-1} (0.1 ppm). The primary sources of Cr(VI) contamination are the metal finishing industries dealing with the welding of stainless steel and chrome plating. It is well known that hexavalent chromium enhances the risk of lung cancer via chronic inhalation.[14,19] However, Cr(III) is relatively inert and much less soluble in water.[14,20,21] Therefore, changes in oxidation state is an effective route to affect chromium solid/solution partitioning and subsurface migration rates. Researchers have used some functionalized materials to reduce Cr(VI), such as mesoporous silica[22] and a combination of ferrous sulfate and sodium dithionite,[23] Pd nanoparticles (NPs)-supported mesoporous TiO_2,[24] and so on. But the cost is very high. An easy method of Cr(VI) reduction by formic acid (FA) using Pd NPs as a catalyst has been reported by Sadik et al.[25,26] The most benefit is in that its oxidation product of FA is CO_2 and no secondary pollution. The special d^1 electronic configuration of Mo^V centers in $\{P_4Mo_6\}$ unit prompt us to further study their catalytic activity for electronic transfer reaction. In this work, hybrids **1-4** were tested for the reduction of toxic Cr(VI) to nontoxic Cr(III) using FA as a reducing agent at low temperatures. Experiment results show that this type of hybrids is active and has good catalytic performance for Cr(VI)→Cr(III). It is very significant to explore the noble-metal-free catalyst for wastewater remediation. The pursuit of more environmentally friendly and economical catalytic systems is still the most important work as well as a challenge.

2. Experimental section

2.1 Materials and measurements

All the reagents were commercially purchased and used without further purification. Hydrothermal synthesis was carried out with a 20 mL Teflon-lined autoclave under autogenous pressure. The reaction vessels were filled to approximately 70% of their volume capacity. Elemental analysis of C, H, N were carried on a Perkin-Elmer 2400CHN elemental analyzer. FTIR spectra were recorded in KBr pellets with a FTIR-8900 IR spectrometer in the range of 400-4000 cm^{-1}. TG analyses were performed on a Perkin-Elmer Pyris Diamond TG/DTA instrument in flowing N_2 with a heating rate of 10 °C min^{-1}. UV spectra were measured by U3010 UV-visible spectrophotometer (Shimadzu). Cyclic voltammograms (CV) were recorded with a 384B polarographic analyzer. A CHI 660 Electrochemical Workstation controlled the electrochemical measurements and data collections. The data were obtained with a conventional three-electrode system: the working electrode was a modified CPE, the reference electrode was a SCE (saturated calomel electrode) electrode, and the counter electrode was Pt gauze. All potentials were measured and are reported *vs*. SCE.

2.2 Synthesis of hybrids 1-4

A mixture of $CoCl_2 \cdot 6H_2O$ (0.09 g, 0.37 mmol), bpp (0.03 g, 0.15 mmol), $Na_2MoO_4 \cdot 2H_2O$ (0.24 g, 3.31 mmol), H_3PO_4 (0.5 mL, 7.5 mmol), H_2O (8 mL, 0.72 mmol), was stirred for 30 min, and the pH was adjusted to approximately 1.0 with 2M NaOH. Then it was transferred to a Teflon-lined reactor and kept at 160°C for 5 days. After the reactor was cooled to room temperature at a rate of 8 °C h^{-1}, the pale brown crystals of crystal **1** were obtained, washed with distilled water, and air-dried to give a yield of 60% based on Mo. Elemental anal. calcd. for $C_{78}H_{154}Co_2Mo_{24}N_{12}O_{137}P_{16}$(%): C, 14.7; H, 2.42; N, 2.64. Found(%): C, 14.1; H, 2.84; N, 2.97.

The preparation of hybrid **2** was similar to the method of **1**, except that the pH value was adjusted to 2.1 with 2M NaOH. The red block crystals were obtained. Elemental anal. calcd. for $C_{78}H_{166}Co_6Mo_{24}N_{12}O_{152}P_{18}$(%): C, 13.5; H, 2.40; N, 2.42. Found(%): C, 12.9; H, 2.64; N, 2.78.

The preparation of hybrid **3** was similar to the method of **1**, except that the initial chemical bpp was replaced with mbpy (0.03 g, 0.16 mmol). The red block crystals were obtained. Elemental anal. calcd for $C_{48}H_{90}Co_5Mo_{12}N_8Na_2O_{80}P_8$(%): C, 15.16; H, 2.37; N, 2.95. Found(%): C, 15.91; H, 2.66; N, 2.79.

The preparation of hybrid **4** was similar to the method of **3**, except that the pH value was changed to 2.0 with 2M NaOH. The red block crystals were obtained. Elemental anal. calcd for $C_{48}H_{110}Co_5Mo_{12}N_8Na_2O_{87}P_8$(%): C, 14.65; H, 2.80; N, 2.85. Found(%): C, 14.89; H, 2.65; N, 2.78.

2.3 X-ray crystallographic study of hybrids 1-4

Single crystal data were collected on a Smart Apex CCD diffractometer at 296(2) K with Mo *Kα* monochromated radiation (λ= 0.71073 Å). The structures of **1-4** were solved by direct methods and refined by the full-matrix least-squares methods on F^2 using the SHELXTL crystallographic software package.[27] Anisotropic thermal parameters were used to refine all non hydrogen atoms. Hydrogen atoms attached to carbon atoms were added to their geometrically ideal positions and refined isotropically. Hydrogen atoms attached to nitrogen atoms and some of water molecules were identified from the difference Fourier map and were constrained in the following refining circles. The representive bond lengths and angles in crystals **1-4** are listed in Tables S1-S4, respectively. All the crystal data and structure refinement details for the hybrids **1-4** were listed in Table 1. CCDC-1037833 (for **4**) and 1037834-1037836 (for **1-3**) contain the supplementary crystallographic data for this paper. These data can be obtained free of charge from The Cambridge Crystallographic Data Centre via www.ccdc.cam.ac.uk/data_request/cif.

2.4 Preparation of hybrids 1-4 modified carbon paste electrodes

Hybrids **1**, **2, 3** and **4** modified CPEs (**1-**, **2-**, **3-** and **4-**CPE) were fabricated as follows: graphite powder (0.5 g) and the relevant crystal (0.05 g) were mixed and ground together with an agate mortar and pestle to achieve a uniform and dry mixture. Paraffin oil (0.5 mL) was added to the mixture, while it was stirred with a glass rod. Then the mixture was packed into a glass tube (3 mm inner diameter), and the surface of the mixture was pressed firmly onto weighing paper with a copper rod inserted at the other end of the tube. Electrical contact was established with a copper rod through the back of the electrode.

2.5 Catalysis experiments of Cr(VI) reduction reaction

The catalytic reactions were carried out in a Pyrex reactor of 80 mL capacity performed. A sample of 20 mg hybrid **1** (**2**, **3** or **4**) was dispersed into 50 mL aqueous solution. The concentrations of $K_2Cr_2O_7$ and formic acid are 4.4×10^{-4} M and 4.6×10^{-2} M, respectively. The system was magnetically stirred at 50 °C. At 30, 60, 90, 120, 150, 210 min, a 3 mL aliquot was sampled and

then centrifuged to remove the particles of catalyst. The evolution of absorption spectra due to the reduction of Cr^{6+} to Cr^{3+} has been recorded using UV-visible spectrophotometer, respectively. Spectra of blank experiments in the absence of catalysts were also recorded.

The ionic Equation for the redox reaction is shown in Equation (1).[28]

$$Cr_2O_7^{2-} + 8H_3O^+ + 3HCOOH \leftrightarrow 3CO_2 + 2Cr^{3+} + 15H_2O \quad (1)$$

The conversion of Cr(VI) was calculated from $([C_0]-[C_i])/C_0 \times 100\%$, where $[C_0]$ is the initial concentration and $[C_i]$ is the concentration at each time point.

Table 1 Crystal data and structure refinement details for the hybrids **1-4**.

Compound	**1**	**2**	**3**	**4**
Empirical formula	$C_{78}H_{154}Co_2Mo_{24}N_{12}O_{137}P_{16}$	$C_{78}H_{166}Co_6Mo_{24}N_{12}O_{152}P_{18}$	$C_{48}H_{90}Co_5Mo_{12}N_8Na_2O_{80}P_8$	$C_{48}H_{110}Co_5Mo_{12}N_8Na_2O_{87}P_8$
Formula weight	6368.07	6917.82	3798.95	3931.11
Crystal system	Monoclinic	Orthorhombic	Triclinic	Triclinic
Space group	*P2(1)/c*	*Pnma*	*P-1*	*P-1*
a (Å)	22.970(4)	29.209(11)	13.5095(16)	14.2222(8)
b (Å)	15.784(3)	23.399(9)	14.0897(17)	15.0491(14)
c (Å)	24.183(4)	15.388(6)	15.3417(18)	16.4125(8)
α (°)	90	90	72.7850(10)	105.9200(10)
β (°)	92.228(2)	90	84.827(2)	110.0210(10)
γ (°)	90	90	74.414(2)	101.5370(10)
Volume ($Å^3$)	8761(2)	10517(7)	2686.6(6)	3001.3(4)
Z	2	2	1	1
Density(calculated)(Mg/m^3)	2.414	2.184	2.348	2.175
Absorption coefficient (mm^{-1})	2.106	2.084	2.342	2.105
F(000)	6208	6746	1855	1931
Crystal size (mm^3)	0.19 × 0.17 × 0.15	0.21 × 0.19 × 0.17	0.21 × 0.19 × 0.17	0.23 × 0.19 × 0.17
θ (°)	1.76 -25.01	1.73 - 25.01	1.77 - 25.01	1.80 - 25.01
Reflections collected	40606	46445	13458	14396
Independent reflections ($R_{(int)}$)	15395 [$R_{(int)}$=0.0325]	9504 [$R_{(int)}$ = 0.0327]	9362 [$R_{(int)}$ = 0.0112]	10396 [$R_{(int)}$ = 0.0117]
Max. and min. Transmission	0.729 and 0.677	0.702 and 0.652	0.672 and 0.618	0.699 and 0.625
Data/restraints/parameters	15395 / 0 / 1235	9504 / 0 / 742	9362 / 7 / 838	10396 / 19 / 858
Goodness-of-fit on F^2	1.053	1.055	1.060	1.062
Final *R* indices [$I > 2\sigma(I)$]	R_1 = 0.0467, wR_2 = 0.1377	R_1 = 0.0344, wR_2 = 0.1073	R_1 = 0.0250, wR_2 =0.0682	R_1 = 0.0245, wR_2 = 0.0733
R indices (all data)	R_1 = 0.0494, wR_2 = 0.1401	R_1 = 0.0394, wR_2 = 0.1125	R_1 = 0.0265, wR_2 = 0.0690	R_1 = 0.0265, wR_2 = 0.0747

3. Results and Discussion

3.1 Synthesis

During experiments on the synthesis of new $\{P_4Mo_6\}$-based supramolecular assembly, we have been aware of the effect of reaction conditions on the final products. Transition metal Co^{2+} cation is employed as the linkage unit to construct these $\{P_4Mo_6\}$-based materials. Hybrids **1**–**4** were achieved by changing organic moieties and pH values with the same reaction temperature and time (Scheme 1). The self-assembly reactions of Na_2MoO_4, H_3PO_4, $CoCl_2$, H_2O, and bpp under pH value of 1.0 or 2.0 gave rise to hybrids **1** and **2**. Using mbpy instead of bpp, hybrids **3** and **4** were obtained, respectively. It is noted that the formation of **1-4** appears to involve full reduction of Mo atoms from d^0 to d^1 electronic configuration. The part reduction phenomenon is usually observed under high temperature and pressure of hydrothermal environment, in which organic amine might play a role of reducing agent. Here phosphoric acid plays double roles: to ensure the required amounts of P source for the reaction process and control the pH values of solutions.

3.2 Structural Analysis

Single crystal X-ray diffraction analysis reveals that the basic anionic unit of hybrids **1-4** is built upon hourglass-shape

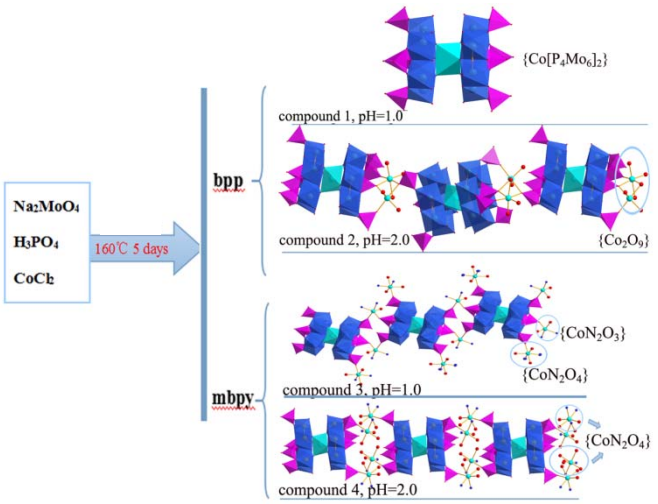

Scheme 1. Schematic representation of the pathways for the formation of **1-4** and their inorganic moieties.

$\{Co[P_4Mo_6X_{31}]_2\}^{n-}$ (X= O or OH) cluster, consisting of two $[P_4Mo^V_6O_{31}]^{12-}$ subunits bridged by one $\{Co^{II}O_6\}$ octahedron. The $\{P_4Mo_6\}$ with a C_3 symmetry has a ring of six edge-sharing $\{MoO_6\}$ octahedra with alternating Mo-Mo single bonds (av. 2.60 Å) and nonbonding Mo…Mo contacts (av. 3.50 Å) (Fig. S1). One phosphate group internally embeds itself in the above-

mentioned ring, and the other three phosphate groups externally are anchored on three long Mo…Mo contacts, respectively. The P-O bond distances are in the range of 1.4869(74)~1.5691(54) Å and the angles of O-P-O are from 105.484(3)° to 115.967(28)°. Then, the central transition metal ion Co^{2+} connects two $\{P_4Mo_6\}$ units via three bridging-oxygen atoms between Mo-Mo single bonds to form the sandwich-type $\{Co[P_4Mo_6]_2\}$ cluster. As shown in the side and top views of Fig. S1, it is worth mentioning that the central phosphate groups and the Mo-Mo bonds on the two $\{P_4Mo_6\}$ rings are evenly staggered to each other with an angle of 60º. According to the valence bond calculations,[29] all Mo atoms are in the reduced +5 oxidation state (5.120~5.346), although they are +6 oxidation states in the raw material of MoO_4^{2-}. P and Co atoms are +5 and +2 oxidation states (Tables S5-S7), respectively.

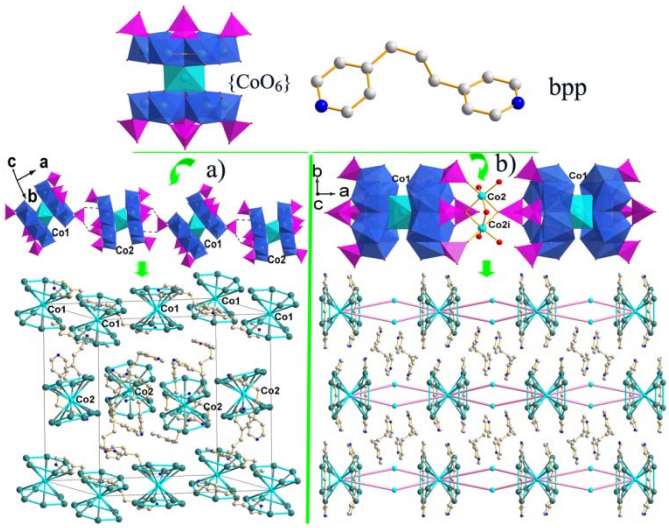

Fig. 1 1D chain-like inorganic moieties and inorganic-organic arrangements of a)**1** and b)**2**. The simplified views show the supramolecular stacking patterns of polyanions and organic cations, in which all O, H and P atoms are invisible. The long solid line bars represent that there are covalent linkages between two metal atoms through oxygen-shared bridging.

3.2.1 Structure description of 1 and 2

By employing the flexible bpp as organic moiety, two supramolecular hybrids of **1-2** were obtained (see Fig. 1). There are extensive and multiple weak interactions existing among inorganic anions and protonated organic cations, including C-H…O, N-H…O, electrostatic and Van der Waals forces. In **1**, Cobalt centers are in octahedral coordination environments to bridge two $\{P_4Mo_6\}$ units via six μ_3-O donors. There are two kinds of crystallograhpically non-identical discrete polyanions: Co(1)- and Co(2)-centered $\{Co[P_4Mo_6]_2\}$ clusters (see Fig. S2). The Co(1)-O bond lengths are of 2.1569(44) Å × 2, 2.1204(46) Å × 2, 2.2024(47) Å × 2, while the Co(2)-O bond lengths of 2.1844(44) Å × 2, 2.1463(47) Å × 2, 2.1219(46) Å × 2, respectively. Two types of discrete $\{Co[P_4Mo_6]_2\}$ polyoxoanions alternately form a 1D chain-like anionic supramolecular structure in a head-to-tail way through O-H…O hydrogen bonding interactions (Fig. 1a, Table S8).

By changing pH value of the above reactive solution from 1.0 to 2.0, hybrid **2** was isolated. Different from that in **1**, the anionic moiety presents a one-dimensional chain-like arrangement of $\{Co[P_4Mo_6]_2\}$ clusters covalently joined to together through $\{Co_2O_5\}$ groups. In addition, one free HPO_4^{2-} anion is also observed (Fig. S3). There are two types of crystallographically independent cobalt atoms Co(1) and Co(2), presenting different octahedral coordination environments. Co(1) locates at the center of $\{P_4Mo_6\}_2$ dimers with Co–O bonds lengths of 2.1403(33) Å × 2, 2.1374(33) Å × 2, and 2.1832(47) Å × 2. Apart from three coordinated water molecules, Co(2) octahedron shares the remaining three vertexes (O(27), O(33), O(20)) with three $\{PO_4\}$ tetrahedra belonging to two different $\{Co[P_4Mo_6]_2\}$ clusters. The Co(2)-O bond distances vary in the range of 2.0336(50)~2.2254(47) Å. Two face-shared Co(2) octahedra as connecters covalently link $\{Co[P_4Mo_6]_2\}$ to form an infinite 1D inorganic chain (Fig. 1b). The adjacent inorganic chains are parallel with each other and are surrounded by organic bpp cations, and finally form the 3D supramolecular network of **2** by hydrogen bonding interactions (Fig. 1b). Some typical hydrogen bonds are shown in Table S9.

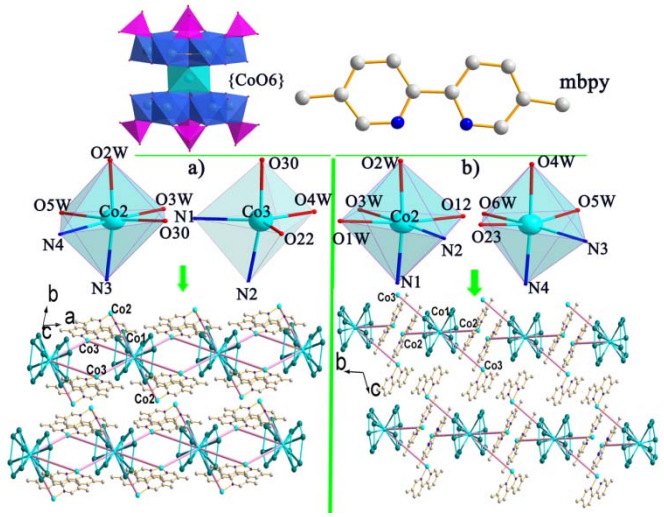

Fig. 2 The structural units of hybrids a)**3** and b)**4**. Views showing the polyhedral coordination environments of cobalt atoms. The simplified draws show the supramolecular stacking of polyanions and organic cations, in which all O, P, H and part C, N atoms are invisible for clarity. The long solid line bars represent that there are covalent linkages between two metal atoms through oxygen-shared bridging.

3.2.2 Structure description of 3 and 4

By employing the rigid and chelated mbpy ligand as organic moiety, two polymorphs **3-4** were isolated. Two crystals consist of $\{Co[P_4Mo_6]_2\}$ clusters peripherally modified by Co-mbpy groups (Fig. 2). There are three crystallographically distinct Co centers in the structure of **3**. The central Co(1) bridges two neighboring hexamer $\{P_4Mo_6\}$ units via six μ_3-O atoms with Co–O bond lengths of 2.1451(25) Å × 2, 2.1532(20) Å × 2, and 2.1463(29) Å × 2, respectively; the pendent Co(2) exhibits octahedral $\{CoO_4N_2\}$ [4+2] coordination geometry and is coordinated by three water molecules (O(3w), O(2w) and O(5w)), one oxygen atom O(30) of $\{PO_4\}$ group and two nitrogen donors from mbpy ligand; the bridging Co(3) adopts square-pyramidal $\{CoO_3N_2\}$ [3+2] coordination geometry and is surrounded by two oxygen atoms (O(31) and O(22)) of two $\{PO_4\}$ groups (P(2) and P(4)) belonging to two different $\{Co[P_4Mo_6]_2\}$ units, one water molecule O(4w) and two nitrogen donors from mbpy ligand. As shown in Fig. 2a, neighboring $\{Co[P_4Mo_6]_2\}$ clusters are doubly bridged by Co(3) octahedra into an infinite 1D inorganic chain-like structure. All the adjacent inorganic chains are parallel with each other, and

further form the 3D supramolecular network via hydrogen bonds and π…π stacking interactions. Some typical hydrogen bonding distances are also shown in Table S10.

By increasing pH value of the reactive solution to 2.0, hybrid **4** is obtained and consists of the similar ingredients to **3** (Fig. S4). There are also three crystallographically distinct Co atoms in the structure of **4**. The central Co(1) bridges two $\{P_4Mo_6\}$ units with Co–O bonds of 2.1378(24) Å × 2, 2.1170(31) Å × 2, 2.1947(28) Å × 2. While the pendant Co(2) and Co(3) exhibit octahedral $\{CoN_2O_4\}$ [2+4] coordination geometry, that the environments include three water molecules (O(1w), O(2w) and O(3w) for Co(2); O(4w), O(5w) and O(6w) for Co(3)), one oxygen atoms (O(12) for Co(2); O(23) for Co(3)), and two nitrogen donors from mbpy (Fig. 2b). Differently, the Na-O interactions, instead of Co polyhedra in **3**, link neighboring $\{Co[P_4Mo_6]_2\}$ clusters into the infinite 1D inorganic chain (Fig. S5). Furthermore, hydrogen bonding and aromatic π…π stacking interactions stabilize the 3D supramolecular framework of **4** (Table S11).

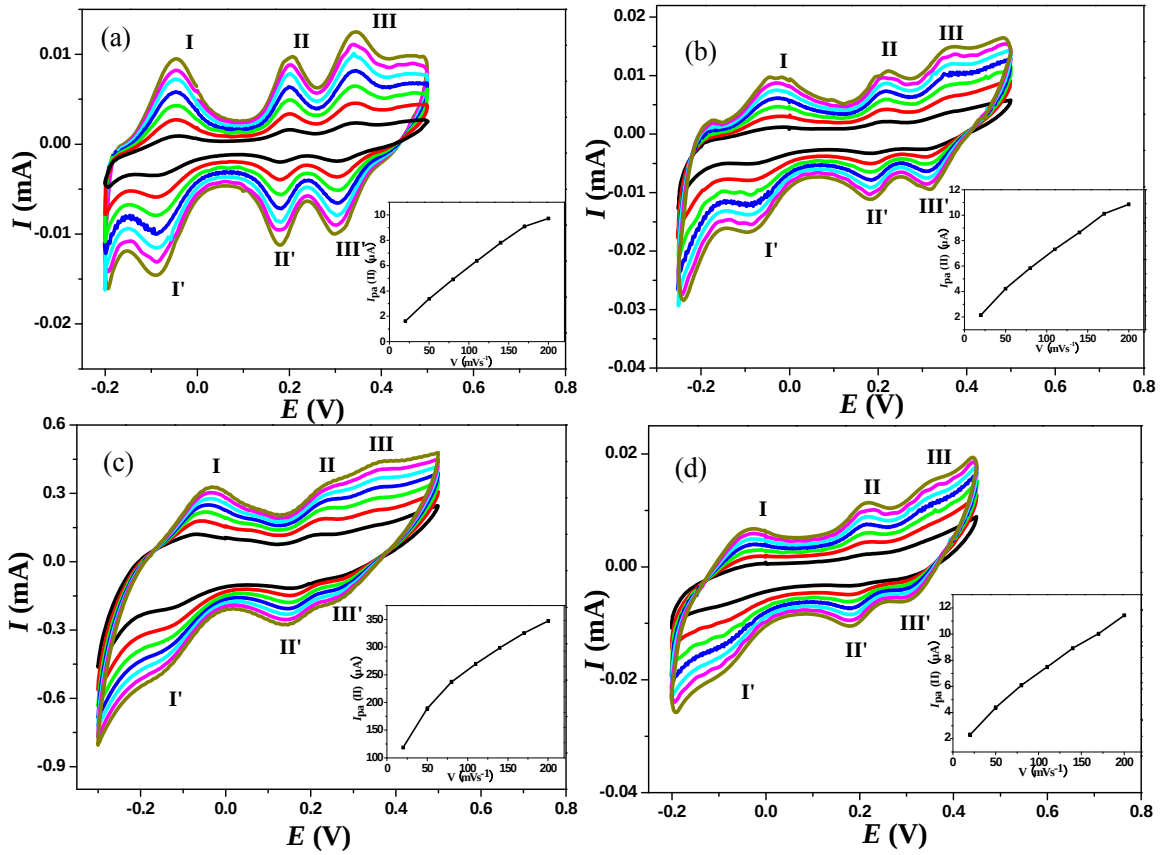

Fig. 3 Cyclic voltammograms of (a) **1**-CPE, (b) **2**-CPE, (c) **3**-CPE, and (d) **4**-CPE in the 1.0 M H_2SO_4 solution at different scan rates (from inner to outer: 20, 50, 80, 110, 140, 170, 200 mV s^{-1}). Potentials *vs*. SCE. (Insert plots: the dependence of anodic peak II currents on scan rates.)

3.3 Characterization

3.3.1 FT-IR spectra

The IR spectra of **1-4** have been recorded between 4000 and 400 cm^{-1}, as shown in Fig. S6a. All four hybrids exhibit characteristic peaks of the $\{P_4Mo_6\}$ polyoxoanion: the characteristic bands in the range of 680-750 cm^{-1} are attributed to ν(Mo–O–Mo) vibrations; strong peaks at 956-970 cm^{-1} are due to ν(Mo=O) vibrations; the ν(P–O) vibration ranges from 1033-1178 cm^{-1}. Small shifts in the wavelengths of $\{P_4Mo_6\}$ characteristic peaks may be due to the different coordination environments in four hybrids. The broad bands at 2781-3437 cm^{-1} are associated with C-H, N-H and O-H bending and stretching vibrations, further proving that there is extensive hydrogen bonding interactions among the supramolecular framework of crystals. Strong peaks at 1480-1640 cm^{-1} are assigned to C–C and C–N stretches of organic amines such as bpp in **1-2** (1505 and 1637 cm^{-1}) and mbpy in **3-4** (1480 and 1635 cm^{-1}), respectively.

3.3.2 TG analysis

Thermogravimetric analyses of crystals **1-4** were investigated under N_2 atmosphere from 20 to 800 °C, and the TG curves are shown in Fig. S7. The results show that the main structures of **1-4** are stabilized up to *ca.* 310°C. TG curve of hybrid **1** displays two weight loss steps: the first weight loss of 3.39% (calc. 3.67%) in the temperature range of 27-231°C corresponds to the loss of lattice water; the second weight loss from 315 to 784°C is attributed to the decomposition of bpp molecule (weight loss: exp. 8.9%, calc. 9.3%). TG curve of **2** indicates that its weight loss can also be divided into two distinct stages: the first weight loss of 7.79% (calc. 8.30%) at 28-306°C corresponds to the loss of lattice water; the second weight loss is attributed to decomposition of composition bpp molecule

from 306 to 785°C. TG curves of **3** and **4** also shows two steps of weight loss: the first is attributed to decomposition of water molecules in 28-317°C for **3** and in 27-190 °C for **4**; the second weight loss is attributed to decomposition of mbpy molecule from 317 to 783 °C for **3** and 310 to 785 °C for **4**, respectively.

3.4 Electrochemical properties

POMs have attracted much interest in electrode modification and electrocatalysis fields because of their ability to undergo a series of reversible multi-electron redox processes. The electrochemical behaviors of crystals **1-4** were investigated with **1**, **2**, **3,** and **4**-CPEs due to their insolubility in water and common organic solvents. The cyclic voltammetric (CV) behaviors in 1.0 M H_2SO_4 aqueous solution at different scan rates were recorded (Fig. 3a-d). There are three pairs of reversible redox peaks I-I', II-II' and III-III' with the half-wave potentials $E_{1/2}$ = (Epa + Epc)/2 at -69.81, 192.19 and 321.18 mV for **1**, -64.58, 201.185 and 340.34 mV for **2**, -102.44, 194.43 and 323.68 mV for **3**, -56.66, 196.015 and 321.57 mV for **4** (scan rate: 140 mV s^{-1}), respectively. Theses redox peaks are ascribed to the redox process of Mo centers.[30] The potential shifts of redox peaks in hybrids **1-4** comparing reported values may relate to the effect of coordinating environments and arrangement modes of polyanions.[31,32] Moreover, The peak potentials change gradually following the scan rates from 20 to 200 mV s^{-1}: the cathodic peak potentials of all four compounds gradually shift toward the negative direction and the corresponding anodic peak potentials shift to more positive values as a result of an uncompensated iR (Ohmic) drop. The net effect is that the peak separation (ΔEp) between the corresponding cathodic and anodic peaks increases, but $E_{1/2}$ almost remains stable. These plots of anodic peak current (II) *vs.* scan rates (see insert plots in Fig. 3) indicate that the redox processes of CPEs are surface-controlled. It is also noteworthy that **1-4**-CPE possesses the high stability. When the potential range is maintained between +0.5 and -0.3V, the peak currents remain almost unchanged over 300 cycles at a scan rate of 140 mV s^{-1} (see Fig. S8).

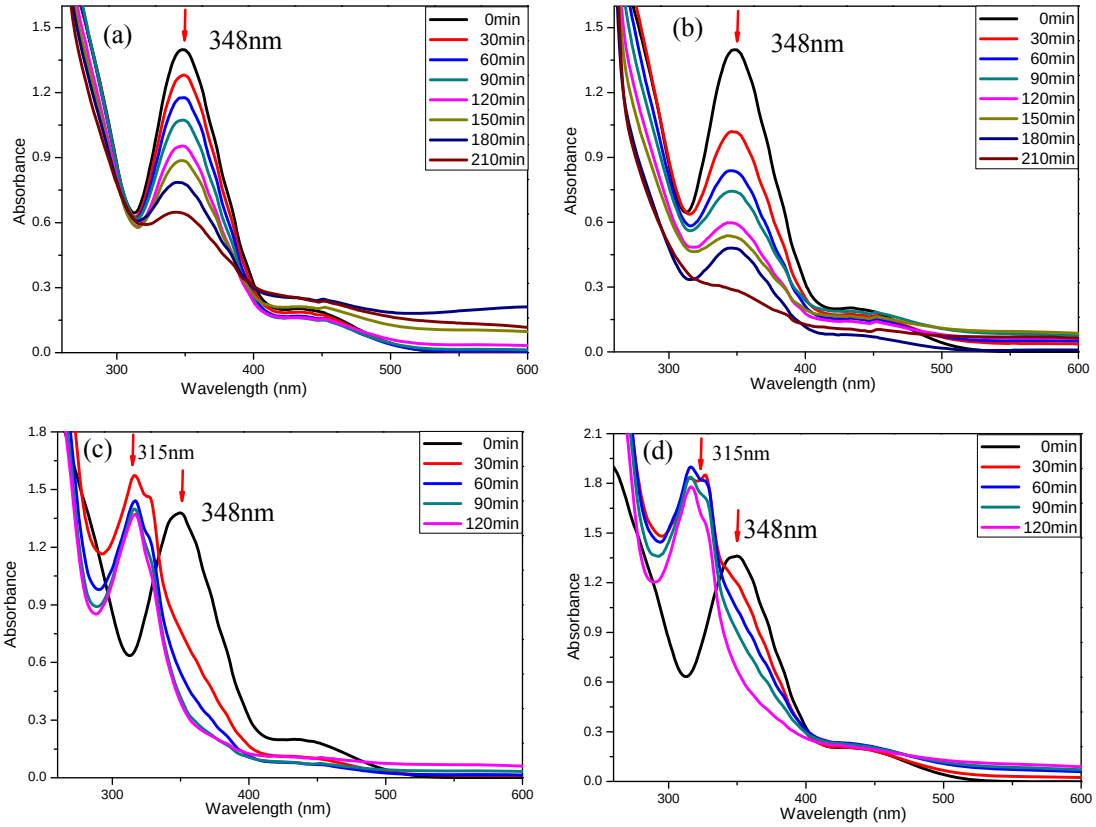

Fig. 4 Successive UV-visible absorption spectra for aqueous solutions of the catalytic Cr(VI) reduction using excess of formic acid at 50 °C under the presence of crystals **1**(a), **2**(b), **3**(c) and **4**(d).

3.5 Catalytic experiments

The reversible electrode potentials and large exposed anionic surfaces of highly reduced hourglass-shape clusters in **1-4** motivate us to further study their catalytic performance for electron transfer reaction. Since hexavalent chromium (Cr(VI)) is an ubiquitous toxic pollutant in the aquatic environment, we take it as a model system to evaluate the catalytic activity of **1-4**. Hybrids **1-4** were used in a study of the catalytic reduction of Cr(VI) to Cr(III) using FA as the reducing agent. Potassium dichromate ($K_2Cr_2O_7$) is chosen as a representative Cr(VI) source. Generally, the reaction is not performed under ambient conditions. It can be found that the reduction rate increases dramatically with the combination of crystals **1-4** in the solution, indicating that these crystals are active for the

reduction of Cr(VI) in the presence of excess FA at 50 °C. As shown in Fig. 4, the characteristic absorption peaks of Cr(VI) ions at 348 nm were gradually decreased with increasing reaction time, as judged by rapid disappearance of the characteristic yellow color (Fig. 5(a), (b)), confirming the reduction of Cr(VI) to Cr(III). Addition of excess sodium hydroxide to the resulting solution led to the formation of a green solution, indicating that Cr(VI) had been reduced to Cr(III).[33-34] In order to study the catalytic nature, the blank experiment of Cr(VI) in the absence of crystal was also carried out. It was obvious to see that the characteristic peak intensity of Cr(VI) at 348 nm was almost constant at 50 °C during a long period of 150 min (Fig. S9). These results indicate clearly that hybrids **1-4** are much active for Cr(VI)→Cr(III) (Fig. 5).

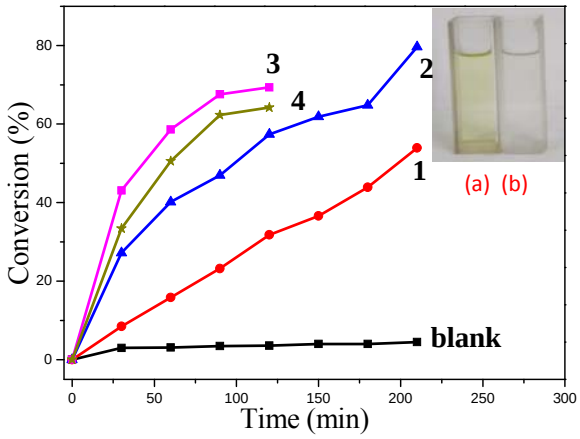

Fig. 5 Plots of the conversion(%) of Cr(VI) *vs*. time with the presence of crystals **1-4** at 50 °C. The inset picture is the color changes of solutions before (a) and after (b) catalytic reaction.

It is worth mentioning that, following the gradual decreasing of absorption peak of Cr(VI) at 348 nm, a new peak at 315 nm is becoming more and more apparent with the addition of **3** or **4** as catalysts. A speculation is that the crystal may be partly soluble in formic acid ascribing to organic component mbpy. We further tested the UV spectra of free mbpy ligand and hybrid **4** in formic acid, respectively (Fig. S10). Both present the strong absorption peaks in *ca*. 310 nm in two experimental curves, verifying the above-mentioned speculation. In addition, the free bpp and mbpy have also been used as catalysts into this system. As shown in Fig. S11, experimental results indicated that both of them have no effect on the reduction of hexavalent chromium. Through these experimental results above-mentioned, one can draw a conclusion that crystals do not decomposed but just partially dissolved in the solution during the reaction process, which is probably affected by high temperature. A comparison between the experimental results of **1-2** and **3-4**, leads one to the conclusion that crystals **3-4** show a higher catalytic performance for the reduction reaction than **1-2**. The reasonable explanation is that the mild solubility of **3-4** just facilitates the catalytic process changing from heterogeneous to homogeneous.

In this system, the FA not only acts as the reducing agent, but maintains the pH of the reaction mixture. To confirm the dual role of HCOOH, an experiment was conducted on the reduction of Cr(VI) by using $Na_2S_2O_3$ and C_2H_5OH as reducing agents, respectively. The pH values of the reaction mixtures were stabilized to within neutral condition. As shown in Figs. S12-13, the reduction process of Cr(VI) were not observed whether or not the presence of crystal **4**. Hence, it is clear that both $Na_2S_2O_3$ and C_2H_5OH had no significant power to reduce Cr(VI) at the current condition.

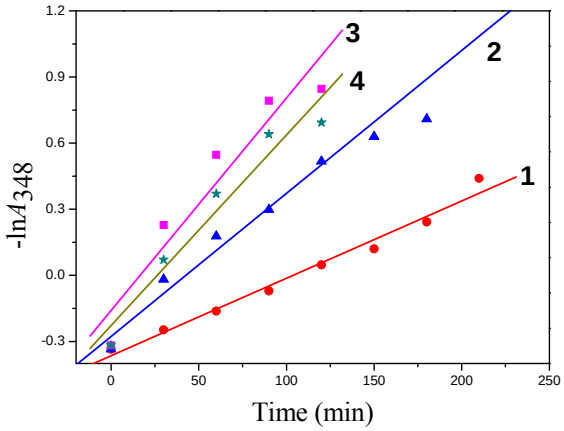

Fig. 6 The pseudo-first-order plots of $-\ln A_{348}$ (absorbance at 348 nm) with time for the Cr(VI) reaction.

The reduction of Cr(VI) to Cr(III) followed pseudo-first-order kinetics as the concentration of HCOOH was taken in excess as compared to Cr(VI). As shown in Fig. 6, the apparent rate constant (K_{app}) was calculated by plotting the negative logarithm of absorbance (at λ = 348 nm) with respect to time (*i.e.*, $-\ln A_{348}$ *vs*. *t*). We found that the high rate constant values of K_{app}= 3.51 × 10^{-3} min^{-1} for crystal **1**, 6.49 × 10^{-3} min^{-1} for **2** in 150 min, and 9.64 × 10^{-3} min^{-1} for **3** and 8.64 × 10^{-3} min^{-1} for **4** in 100 min were observed for these systems, respectively. It is worth mentioning that the K_{app} constant of crystal **3** is better than the other three samples. It should be emphasized that these are apparent rate constants used for comparative purposes amongst these materials and will depend on the reaction conditions employed. In contrast to the precious metal Pd and Pt NPs as catalysts, these K_{app} constants are of the same order of magnitude. However, this kind of hybrids is cheaper and easier to prepare, and more importantly, can be structurally designed and optimized. Some facts can be found: i) the mbpy-containing structures (**3** and **4**) have better activity than bpp-modified structures (**1** and **2**); ii) it is a multiple-effect of heterogeneous and homogeneous catalytic reaction for **3-4**; iii) the extending structural topologies and cobalt coordination environment are related to the catalytic performance of **1-4**.

To experimentally verify the reaction observed is truly catalytic process, a blank experiment was designed and performed. The absorbance of solutions initially containing 4.4 × 10^{-4} M $K_2Cr_2O_7$ was monitored as a function of time in the presence and absence of FA and hybrid **1** at 50 °C. Fig. 7 reported the results of this experiment performed in aqueous solution. Curve consists of two stages: the concentration of Cr(VI) almost remains unchanged with the presence of only hybrid **1** during 150 min, indicating that there is no observable reaction between hybrid **1** and Cr(VI). When the reductant HCOOH is added, the rapid decrease in $[Cr^{VI}]_{aq}$ with the duration of the experiments means that Cr^{VI} is quickly transformed to Cr^{III}. These results suggest that hybrid **1** itself can not markedly adsorb as well as not reduce $K_2Cr_2O_7$, but only catalyze the reduction reaction of Cr(VI) with HCOOH. Our preliminary data clearly showed that the 3D

supramolecular assemblies of Co-containing POMs can be used as candidates for Cr(VI) reduction. Because the reduction step is an electro-transfer process, reported work also confirmed that the catalysis reaction occurred through the electron transfer at the noble metal NPs surface.[35] Highly reduced polyanion $\{Co[P_4Mo^V_6]\}$ cluster might be more conducive to electron transfer in a much faster manner. Much work needs to be done for making clear this fact in the removal of Cr(VI) from wastewater for environmental remediation.

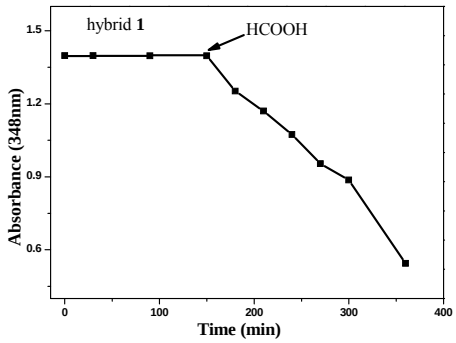

Fig. 7 A controlled experiment showing the reduction of Cr(VI) catalyzed by hybrid **1** as a function of time in two stages at 50 °C: FA-free solution in the first 150 min; adding FA into the solution to run the reduction reaction.

During the course of catalytic experiments, these POM-based supramolecular frameworks maintain higher catalytic activity and structural stability. The catalyst can be easily separated after the reaction and resused several times. Under the same conditions, the catalytic reaction was performed multiple times using the same sample of **1**. It is found that the conversion rates of Cr^{VI} become almost the same with the increase of repeated cycles (see Fig. 8). The results showed that the conversion(%) of Cr^{VI} only fell by 4% after four times cycling experiments. IR spectra of the fresh and used catalysts are measured to check the structures of crystals **1-4** (Fig. S6b). The characteristic peaks illustrate that the skeleton of the polyanion still remains intact after catalytic reaction. Furthermore, X-ray photoelectron spectra are measured to monitor the oxidation state of Mo in compound **1** before or after catalysis (Fig. S14). The results show that Mo^V are stable in its reduced oxidation state (+5).

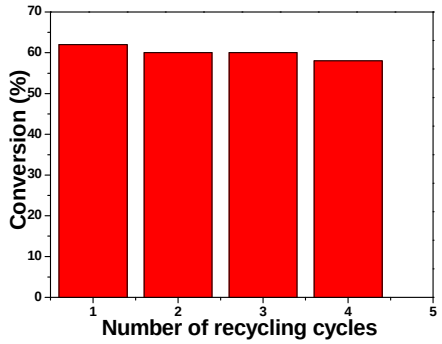

Fig. 8 Four consecutive cycles for catalytic reduction of Cr(VI) using the same sample of hybrid **1**.

4. Conclusions

In this paper, four hybrids consisting of reduced molybdophosphates have been synthesized and structurally characterized. The successful preparation of **1-4** fully depend on changing organoamines and the pH values of solutions, showing that both of them are the critical factors in controlling the final crystal structure. The introduction of Co centers into crystal frameworks can adjust the electrochemistry property and improve the reversibility of redox reaction. This kind of hybrids exhibits good performance as heterogeneous catalysts for the reduction reactions of highly toxic aqueous chromium(VI), and has the potential to replace costly Pd and Pt NPs used in the environmental remediation for Cr(VI)-containing wastewater. These hybrid systems are cheaper and easily obtained, in particularly, they can be structurally designed to optimize their property and application in environmentally friendly catalytic reaction. It is expected to construct diverse new materials with different types of active POMs for their wide applications in the future. Much work on the hybrids and reaction systems in our group is underway.

Acknowledgements

This work was supported by the National Science Foundation of China (21341003), and the Natural Science Foundation of Hebei province (B2011205035).

Notes and references

[a] College of Chemistry and Material Science, Hebei Normal University, Shijiazhuang, 050024, China. E-mail: hanzg116@126.com.

Electronic Supplementary Information (ESI) available: [details of any supplementary information available should be included here]. See DOI: 10.1039/b000000x/

References

1 C. L. Hill (Guest Ed.), *Chem. Rev.*, 1998, **98**, 1.
2 M. T. Pope and A. Müller, *Polyoxometalate Chemistry From Topology via Self-Assembly to Applications*, Kluwer Academic Publishers, Dordrecht, The Netherlands, 2001.
3 M. T. Pope and A. Müller, *Angew. Chem., Int. Ed. Engl.*, 1991, **30**, 34.
4 D. L. Long, E. Burkholder and L. Cronin, *Chem. Soc. Rev.*, 2007, **36**, 105.
5 A. Proust, R. Thouvenot and P. Gouzerh, *Chem. Commun.*, 2008, 1837.
6 Y. Ma, Y. G. Li, E. B. Wang, Y. Lu and X. X. Xu, *J. Mol. Struct.*, 2006, **791**, 10.
7 Y. S. Zhou, L. J. Zhang, X. Z. You and S. Natarajan, *J. Solid State Chem.*, 2001, **159**, 209.
8 X. Zhang, J. Q. Xu, J. H. Yu, J. Lu, Y. Xu, Y. Chen, T. G. Wang, X. Y. Yu, Q. F. Yang and Q. Hou. *J. Solid State Chem.*, 2007, **180**, 1949.
9 K. Yu, W. L. Chen, B. B. Zhou, Y. G. Li, Y. Yu, Z. H. Su, S. Gao and Y. Chen, *CrystEngComm*, 2011, **13**, 3417.
10 H. Zhang, K. Yu, J. H. Lv, C. M. Wang, C. X. Wang and B. B. Zhou, *J. Solid State Chem.*, 2014, **217**, 22.
11 D. W. Yan, J. Fu, L. Zheng, Z. B. Zhang, Y. Xu, X. L. Zhu and D. R. Zhu, *CrystEngComm.*, 2011, **13**, 5133.
12 C. Streb, D. L. Long and L. Cronin, *CrystEngComm*, 2006, **8**, 629.
13 (a) Z. G. Han, X. Q. Chang, J. S. Yan, K. N. Gong, C. Zhao and X. L. Zhai, *Inorg. Chem.*, 2014, **53**, 670; (b) J. S. Yan, X. F. Zhao, J. Huang, K. N. Gong, Z. G. Han and X. L. Zhai, *J. Solid State Chem.*,

2014, **211**, 200; (c) J. S. Yan, K. N. Gong, X. L. Xue, X. L. He, C. Zhao, Z. G. Han and H. T. Yu, *Eur. J. Inorg. Chem.*, 2014, 5969.
14 A. Dandapat, D. Jana and G. De, *Appl. Catal., A*, 2011, **396**, 34.
15 O. A. Sadik, N. M. Noah, V. A. Okello and Z. Y. Sun, *J. Chem. Educ.*, 2014, **91**, 269.
16 M. Yadav and Q. Xu, *Chem. Commun.*, 2013, **49**, 3327.
17 Y. L. Guo, D. Wang, X. Y. Liu, X. D. Wang, W. S. Liu and W. W. Qin, *New J. Chem.*, 2014, **38**, 5861.
18 H. Y. Li, T. S. Wu, B. Cai, W. G. Ma, Y. J. Sun, S. Y. Gan, D. X. Han and L. Niu, *Appl. Catal. B*, 2015, **164**, 344.
19 P. Kaszycki, H. Gabrys, K. J. Appenroth, A. Jaglarz, S. Sedziwy, T. Walczak and H. Koloczek, *Plant, Cell Environ.*, 2005, **28**, 260.
20 H. C. Lukaski, *Annu. Rev. Nutr.*, 1999, **19**, 279.
21 J. B. Vincent, *Accounts Chem. Res.*, 2000, **33**, 503.
22 N. Shevchenko, V. Zaitsev and A. Walcarius, *Environ. Sci. Technol.*, 2008, **42**, 6922.
23 R. Ludwig, C. Su, T. R. Lee, R. T. Wilkin, S. D. Acree, R. R. Ross and A. Keeley, *Environ. Sci. Technol.*, 2007, **41**, 5299.
24 S. Zheng, L. Gao, Q. Zhang and J. Sun, *J. Solid State Chem.*, 2001, **162**, 138.
25 M. A. Omole, I. O. K'Owino and O. A. Sadik, *Appl. Catal. B*, 2007, **76**, 158.
26 B. Koushik, M. Arnab, K. M. Manish and D. Goutam, *Langmuir*, 2014, **30**, 3209.
27 G. M. Sheldrick, SHELXTL-97, Programs for Crystal Structure Refinement, University of Göttingen, Germany, 1997.
28 T. Vincent and E. Guibal, *Ind. Eng. Chem. Res.*, 2002, **41**, 5158.
29 I. D. Brown and D. Altermatt, *Acta Crystallogr., Sect. B*, 1985, B**41**, 244.
30 X. L. Wang, C. Xu, H. Y. Lin, G. C. Liu, S. Yang, Q. Gao and A. X. Tian, *CrystEngComm*, 2012, **14**, 5836.
31 X. L. Wang, J. J. Cao, G. C. Liu, H. Y. Lin and A. X. Tian, *Inorg. Chim. Acta*, 2013, **402**, 6.
32 Z. G. Han, Y.L. Zhao, J. Peng, Q. Liu, E. B. Wang, *Electrachim. Acta*, 2005, **51**, 218.
33 M. A. Omole, I. O. K'Owino and O. A. Sadik, *Appl. Catal. B.*, 2007, **76**, 158.
34 E. Abass, M. Alireza and V. Reza, *Am. J. Appl. Sci.*, 2005, **2**, 1471.
35 C. X. Yang, J. H. Meldona, B. Lee and H. Yi, *Catal. Tod.*, 2014, **233**, 108.